The Analysis on Dynamic Responses of Bridge Pier due to Vehicle Impact

Mey Met[1], Guichun Wang [1], Ameen Topa[2,3]

[1]School of Civil Engineering, Zhengzhou University, Zhengzhou 450001, Henan Province, China
[2]Institute of Transportation Infrastructure, Universiti Teknologi PETRONAS, Seri Iskandar, 32610, Malaysia
[3]Faculty of Ocean Engineering Technology and Informatics, Universiti Malaysia Terengganu, Kuala Terengganu, 21030, Malaysia

ABSTRACT: *This paper mainly used finite element technology to analyze the responses of reinforced concrete bridge piers subjected to vehicle collision. A single vehicle-pier collision was established by using LS-DYNA. The material constitutive was validated. The pier was considered fixed at the bottom end for any case, and two restraint conditions were considered at the upper end, one was fixed, and another was the hinge. For the hinge condition, to analyze the effect of superstructure load on dynamic responses of the pier, the axial compressive loads P_0 of 5% and 10% of the column's axial load compressive capacity were exerted, respectively. The reliability of the finite element model was validated. Parametric studies were carried out to analyze the effect of preload induced by implicit dynamic relaxation, compressive axial load, boundary condition at the top end, and impact velocity. Based on the simulation result, the dynamic responses of the pier for different boundary conditions were quite different, and it was unconservative to study vehicle-pier collision without considering the axial compressive load due to mass superstructure.*

I. INTRODUCTION

Vehicle collisions with bridge piers have been increasingly reported. Some vehicle-pier collision accidents result in severe damage to the bridge structure, loss of human lives, and affect the economy. The China equivalent static method was adopted in JTG D60-2015, which stipulates that the impact load limit of urban piers was 1000 kN [1]. Abutments and piers within 9.144 m of the roadway must be considered for the extreme event of a vehicle collision, according to the current design standard provided by the American Association of State Highway and Transportation Officials (AASHTO) Load and Resistance Factor Design (LRFD) Bridge Design Specifications (2012) [2]. If a bridge was discovered to be vulnerable to car collisions, it must be constructed to either redirect or absorb the impact force or offer structural resistance. The structure shall be constructed for a 2700 kN single point load delivered to the pier at a height of 1.524 m above the ground and at an angle of incidence from 0 to 15 degrees with the pavement edge in a horizontal plane. This proposal, on the other hand, was based on experimental testing with a single semi-tractor-trailer colliding at 50 mph with a rigid pier [3]. When constructing a bridge pier with varied design specifications that may be subjected to diverse loading situations such as fluctuating vehicle mass and velocity, this offers a lot of space for error. AASHTO's design specifications, according to a past study, underestimate the demand projected on the bridge pier due to crash loading [4], [5]. This raised concerns about the safety of the current bridges in use. The rate of bridge failure and trends in the United States were explored in studies and found that the impact failures were the second most common cause of failure, behind hydraulic failures, according to both studies [6], [7]. Because there are so many vehicles and bridges in use, there is a greater chance of a collision. Concrete spalling is common at the impact point of piers due to the impact of light domestic cars. The impact piers will shear under the weight of big trucks, causing the superstructure to collapse and causing significant economic and property damages. Vehicle collisions in the past have caused considerable damage to the pier, bent cap, foundation system, and superstructure, with the threat of the bridge collapsing completely. A bridge breakdown would have negative economic consequences, represent a threat to public safety, and result in the loss of human life. Direct expenses would include the cost of closure and immediate emergency repairs, particularly if the damaged bridge

is a critical component and traffic circulation is disrupted because of the failure. Many researchers have carried out more in-depth research on the damage mechanism of bridge piers. Different research methods can be roughly divided into three categories: experimental research, theoretical research, and numerical simulation research.

Understanding how a bridge or its components are destroyed during a collision is crucial for determining bridge safety and the impact on the local transportation network. Full-scale verification of impacts on bridge structures is difficult due to the high expense and logistical problems associated with conducting full-scale tests on bridge structures. This method is used in a smaller number of investigations. The number of studies using this method is less. Buth et al. [3] conducted two full-scale impact tests on the pier with a 36t heavy-duty trailer at the speed of 80 km/h. Eccentric impact on rigid piers was the initial set of tests, and the bottom end of the piers was treated as a fully consolidated constraint. The second set of tests was a normal impact test with an eccentricity of zero and a full load of sand in the carriage. The American bridge design code AASHTO-LRFD (1998) amended the bridge collision problem based on these two sets of test results: (1): When bridge piers were not covered by a crashworthy barrier and were within 10 m of the edge of a roadway, the design value of impact force given in the previous code was 1800 kN static force. The result was advised to be revised to 2700 kN in subsequent editions of the specification AASHTO-LRFD (2017). An experimental study on the import of the anti-ram bollard by a truck was carried out by Chen et al (2015) [8] at Hunan University, China. A Dongfeng EQ140 truck to test the impact of a bumper. The truck's net weight was 5.17 t, the anti-collision bar was 6 concrete-filled steel tubular columns with an outer diameter of 0.219 m and a height of 1.3 m, the thickness of the steel tube was 20 mm, the steel tube was filled with C40 concrete, and the impact speed was 43.2 km/h. The collision truck crashed straight into the middle bollard. The truck was damaged severely during impact. Although the static capacity of the bollard was 350 kN, which was one-tenth of the average impact force of 3663 kN, the columns did not undergo large deformation with a residual displacement of 33 mm and a drift ratio of 2.54%. But this test was mainly to measure the anti-collision performance of the anti-collision column and put forward the static design method of the anti-collision column.

Engineers are used to simplifying complex problems. For the problem of contact and collision between objects, the usual method is to simplify the collision model to the single or multi-degree freedom model based on the basic principles of dynamics. Al Thairy (2013)[9] simplified the vehicle bridge collision model as a mass-spring system, which belongs to a single degree of freedom system. The advantage of this model is that the force-displacement relationship is bilinear, and the calculation accuracy is high. However, the model is only for small family cars, but not for heavy trucks. Lin Chen [10] proposed and validated coupled mass-spring-damper (CMSD) model for simulating truck collision on bridge pier and it was used to gain insight into the main parameter affecting the problem. The result showed that the model can be simplified into an equivalent two-degree-of-freedom dynamic system that captures the basic mechanical characteristics of the impact problem.

Numerical simulation technology has been widely used in the study of vehicle impact on bridge piers because of its obvious characteristics of low cost and can use repeatability. El Tawil (2005) [11] used LS-DYNA to establish a refined vehicle bridge coupling model for the first time. The calculation results showed that the peak value of vehicle impact force was greater than the limit value of impact force specified in the old version of the AASHTO-LRFD bridge code (1998), but El Tawil thought that the peak value of impact force was short, and the structure had no time to respond, so it was more appropriate to use the equivalent static value of impact force as the design value of pier anti-collision. Liu (2012) [12] studied the dynamic response of a three-column pier of a three-span simply supported bridge impacted by a truck. Taking the vehicle impact velocity as the parameter, the damage mechanism of the pier after impact is divided into six categories, namely pier erosion, foundation shear, steel bar shedding, pier fracture, pier concrete peeling, and plastic hinge formation. Xu (2017) [13] further simplified the pier bent model from Lui (2012) and still achieved a good result. Xu studied two alternate boundary conditions for pier: a pier bent model with a fixed boundary condition at the top and a pier with fixed top and bottom boundary conditions. It was found that damage modes for the latter two cases were almost the same as those for the pier-bent mode.

II. NUMERICAL FE MODELING
2.1 RC PIER MODLE

The prototype of the finite element bridge pier model with different restraint effects at the top end was shown in Figure 1, and two values of axial load level, ranging from 5% and 10% of the column's axial capacity (P_0) were used to discuss in this paper. The column nominal axial capacity (P_0) was calculated according to the AASHTO-LRFD specification as shown in equation (1) and the design value was listed in Table 1. Concrete in the pier was modeled by solid elements and steel reinforcement was modeled by beam elements. The mesh size of each element is 40 $mm \times$ 40 mm. All the piers were reinforced longitudinally by 1.125% of the cross-sectional area.

$$P_0 = A_s f_y + 0.85 f_c' (A_c - A_s) \tag{1}$$

A_s = The cross-sectional area of longitudinal reinforcement (mm^2)

A_c = The cross-sectional area of the concrete pier (mm^2)

f_y = the yield strength of the longitudinal reinforcement (MPa)

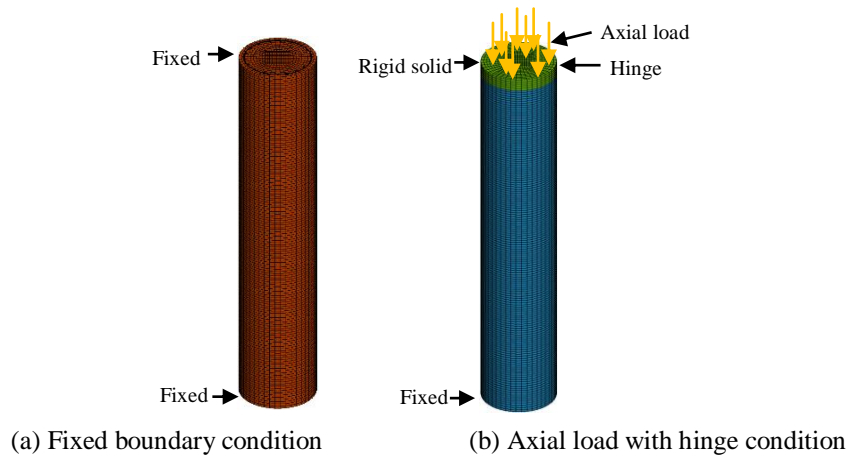f_y' = the cylindrical concrete's unconfined compressive stress (MPa)

(a) Fixed boundary condition　　(b) Axial load with hinge condition

Figure 1 Finite element pier model

Table 1 Design value of RC pier

Pier diameter (mm)	Height (mm)	Concrete compressive strength (MPa)	Yield stress of steel (MPa)	Longitudinal steel (mm)	Hoop steel (mm)
1000	6000	42	420	25	10@150

The impact between vehicle and bridge pier belongs to the category of low-speed impact, so it is more appropriate to use MAT72 and MAT159 as the constitutive model of bridge pier [14]. Material model MAT159 is an elastoplastic damage model for concrete with the strain-rate effect. This model was developed for roadside safety applications such as concrete bridge rails, bridge piers, and portable barriers impacted by vehicles [15]. The default material properties are developed without adequate consideration of the behavior and found the three important parameters: the fracture energy in pure shear (G_{fs}), uniaxial compression (G_{fc}), and tension (G_{ft}) to have a significant influence on the failure mode predicted by the model [16]. The extensive studies to calibrate these parameters found the optimal values were 0.4, 1, and 0.4 times the default values of (G_{fs}), and (G_{ft}) in the MAT 159 card in LS-DYNA, respectively [16]. Equations (2) and (3) are the compression $d(\tau_b)$ and tension damage index $d(\tau_d)$ calculation formulas of MAT 159. The sample input card for MAT 159 is shown in Table 2.

$$d(\tau_d) = \frac{d_{max}}{B} \left[\frac{1+B}{1+B e^{-A(\tau_d - \gamma_{0d})}} - 1 \right] \tag{2}$$

$$d(\tau_b) = \frac{0.999}{D} \left[\frac{1+D}{1+D e^{-C(\tau_b - \gamma_{0b})}} - 1 \right] \tag{3}$$

$$\tau_b = \sqrt{E \varepsilon_{max}^2} \quad , \quad \tau_d = \sqrt{\frac{1}{2} \sigma_{ij} \varepsilon_{ij}} \tag{4}$$

Where d_{max} is the maximum damage value of the element; τ_b, τ_d according to the formula (4), the strain energy of concrete element under tension and compression depends on the stress-strain state of the element, and when the element damage reaches 0.99, the element fails and degenerates; γ_{0d}, γ_{0b} is the initial damage threshold parameter; A, B, C and D are the shape factors in the strain-softening stiffness degradation

The constitutive material model MAT 003 (mat_plastic_kinematic), 2×2 Gauss quadrature, tubular, and beam element was used to simulate the reinforcement behavior because they allow FEM strains to occur, are simple and computationally efficient [17]. Bound-slip effect in the interface between concrete and reinforcement was constrained by using LARANGE_IN_SOLID which simulates the perfect bound behavior. The strain rate affects the stress-strain relation of steel as it affects the speed at which deformation occurs [18]. The material model was used to take the strain rate effects on the dynamic responses of the steel material as shown in Equation (5). The sample input card for MAT 159 is shown in Table 3.

$$\sigma_y = \left(\sigma_0 + \beta E_p \varepsilon_p^{eff} \right) \left[1 + \left(\frac{\dot{\varepsilon}}{c} \right)^{1/p} \right] \qquad (5)$$

Where σ_y is the dynamic yield strength; σ_0 is the yield strength; β is the hardening parameter; E_p is the plastic hardening modulus; ε_p^{eff} is the effective plastic strain; $\dot{\varepsilon}$ is the strain rate; C and P are constant.

In this study, the CONTACT_AUTOMATIC_SURFACT_TO SURFACE (ASTS) was used to define between the vehicle and pier. The static friction coefficient is 0.3 and the dynamic coefficient is 0.2 [19]. The exponential decay coefficient is 0.1 and the viscous damping coefficient is 30 [20]. The soft constraint option (SOFT) is set to 1 to reduce the penetration between the vehicle and the pier; this is recommended when two bodies with dissimilar material and mesh densities encounter one another. Hourglass energy must be inspected in the energy balance of the system and should be kept under 10% as a rule of thumb [21]. To combat this issue, the type_5 (Flanagan_Belytschko with exact volume integration hourglass control) was used with a coefficient 0.05 [22].

Table 2 Sample input card for MAT 159

RO (t/mm³)	NPOT	INCER	IRATE	ERODE	RECOV	ITRETRC	PRED	FPC (MPa)	DAGG (mm)
2.5e-09	1	0	1	1.1	10	0	0	42	10

Table 3 Sample input card for MAT_PLASTIC_KINEMATIC

RO (t/mm³)	E (MPa)	PR	SIGY (MPa)	ETAN (MPa)	BATA	SRC	SRP	FS	VP
7.85e-9	2e5	0.3	420	1500	0	40	5	0.2	10

2.2 VEHICLE FE MODEL

The vehicle model Ford SUT (35,313 elements) was developed by the National Crash Analysis Center of George Washington University (NCAC) [23] and the Federal Highway Safety Administration (FHWA). The vehicle model was widely used in various collision scenarios because of its excellent modeling completion [24]. The vehicle weight 8t and the velocity is 60 km/h, 80 km/h, and 100 km/h were used as vehicle parameters.

III. VALIDATING THE FINITE ELEMENT MODELING

3.1 VALIDATION OF PIER MODEL

The drop weight test conducted by Fujikake [25] was selected as the object, and the corresponding finite element model of the vertical drop weight test was established, as shown in Figure 2. The falling weight was set as a rigid body model, and the contact algorithm between the falling weight and the beam was automatic surface-to-surface contact. The simulation results were compared with the drop weight test data to indirectly verify the rationality of the vehicle bridge coupling model. The section size of the beam in the drop weight test is 250 mm × 150 mm. The aggregate size is 10 mm, and the yield strength of the longitudinal bar and stirrup of D22 is 426 MPa. The beam is fixed on the supporting device without considering the bond slip between the steel bar and the concrete, to limit the out-of-plane displacement of the beam without limiting the rotational freedom of the beam. A 400 kg drop hammer will impact the beam from different heights above the beam. The case selected in this paper is S2222, the diameter of the stirrup and longitudinal bar is 22 mm, and the falling height of the drop hammer is 0.3 m, 0.6 m, 1.2 m, and 2.4 m, respectively.
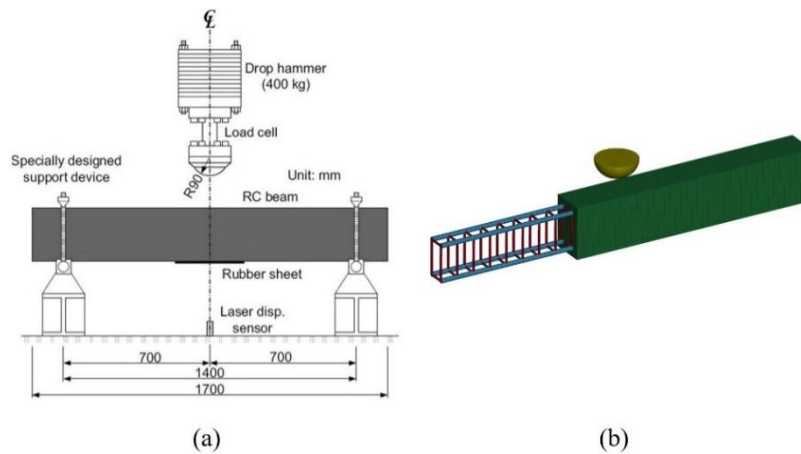
Figure 2 Drop weight test device and FEM model

Figure 3 presents a comparison between the experiment and simulation result of beam S2222 with drop weight of 1.2 m. When the drop height of the hammer is 1.2 m, the peak impact force of the drop hammer is 315 kN, while the peak impact force of the simulation is 331 kN. The error data between the latter and the former is 4.83%. The peak displacement of the experiment is 21.4 mm, while the peak displacement of the simulation is 20.3 mm. The error data between them is 5.14%. Table 4 shows the peak impact force and peak displacement from the experiment and simulation result. The simulation of RC beams impact is shown to be good in agreement with the experimental test, the error between the simulation data and the test is controlled below 10% which is within the acceptable range.
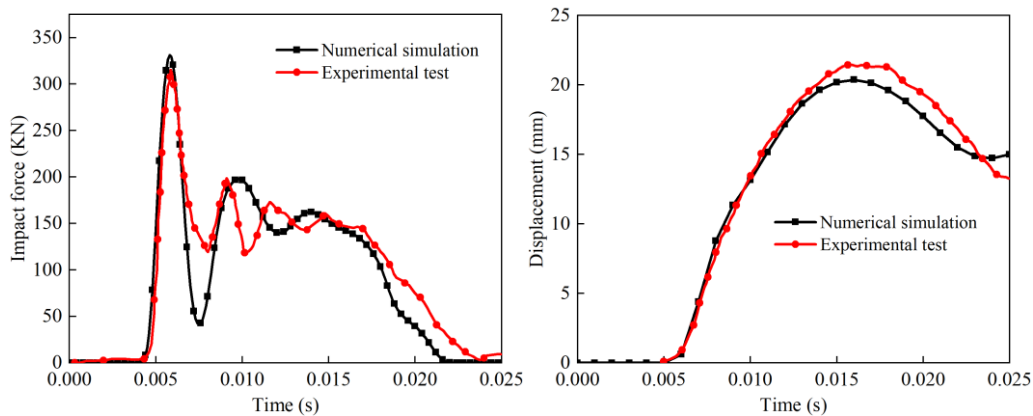

Figure 3 Falling height 1.2 m

Table 4 Peak impact force and midspan displacement

Design beam	Drop height (m)	Peak impact force (kN)		Peak midspan displacement (mm)	
		Experiment	Simulation	Experiment	Simulation
S2222	0.3	210	190	7.3	6
	0.6	272	277	11.2	11.4
	1.2	315	331	21.4	20.3
	2.4	400	380	32.7	34.7

3.2 VALIDATION FORD SUT MODEL

In order to verify Ford F800 reduced model, contact algorithms used and its effectiveness, the truck is crushed on the bridge pier to verify its effectiveness again. This impact velocity is chosen to compare peak impact forces from the simulation results to impact force-time history recorded from the published literature by Lin Chen et al. [26]. Lin Chen studied the response spectrum-based method for calculating the reaction force of a pier subjected to truck collision by using a validated coupled mass-spring-damper (CMSD) model for simulating truck collisions on a bridge pier. Figure 4 shows the comparison of the time history curve of impact force obtained by simulation with the data from Lin Chen. It can be seen from Figure 4 that there is a certain deviation between current FEM simulation results and published results. The first peak impact force of the

current FEM simulation result, Lin Chen's FEM, and CMSD model are 13.3 MPa, 16 MPa, and 14.54 MPa, respectively. Compared with the Lin Chen, FEM, and CMSD model, the error of the former is 16.87% and 8.5%, respectively. The second peak impact force of the current FEM result, Lin Chen's FEM, and CMSD model are 20.73 MPa, 17.21 MPa, and 18.27 MPa, respectively. The error of the current numerical FEM result is 17% and 11.9%, respectively. The time history curve of the first impact force is identical for all cases, and the time history curve of the second impact force for the current simulation result is between those two cases. The analytical results are in the acceptable range of value reported in the published literature that can help verify that model is working correctly.

Figure 4 Comparison of impact force

IV. ANALYSIS OF VEHICLE-PIER COLLISION

4.1 STRESS INITIALIZATION DUE TO AXIAL COMPRESSIVE LOAD

In practical engineering, in addition to its own gravity, the pier also receives the gravity load from the superstructure. The pier which resists axial load capacities is preloaded under gravitational force before the vehicle impact simulation is performed. There are three ways we can use to impose initial gravity loads such as quasi-static transient analysis with mass damping, explicit dynamic relaxation, and implicit dynamic relaxation. In this paper, implicit dynamic relaxation by making two separate runs is used to induce preload due to high computational efficiency. Load curve id name is defined to represent the load on structure as shown in Figure 5 and the gravity acceleration is 9800 mm/s^2.
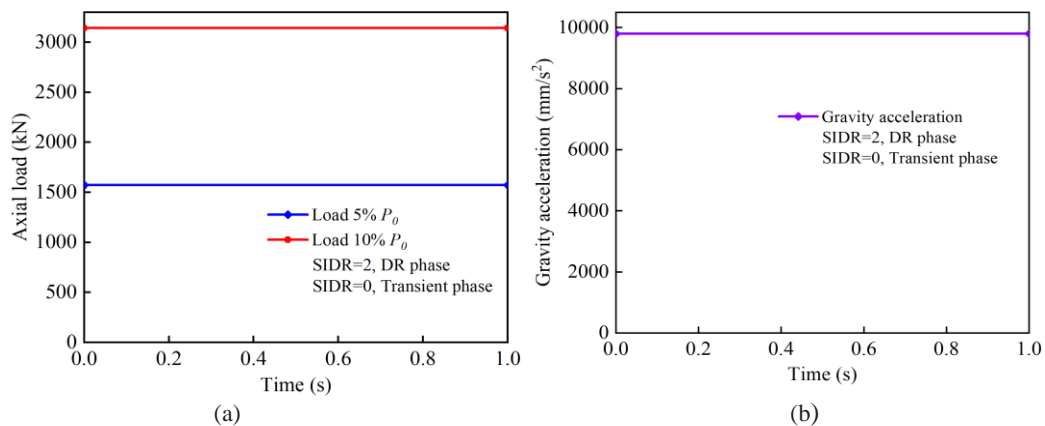

Figure 5 Axial load curve (a), and gravity acceleration (b)

Figure 6 (a) and (b) show the Von Miss Stress of the FEM pier model after stress initialization due to compressive load of $5\%P_0$ and $10\%P_0$. We can see that the structure has already stress in it before simulating the collision impact and this stress affects the result of the dynamic response of the bridge pier.
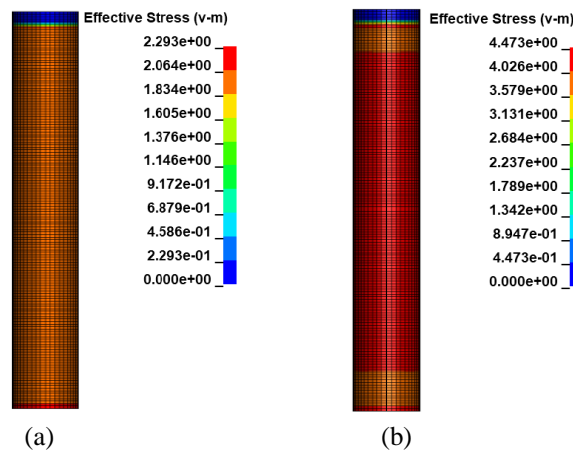
Figure 6 Von miss stress (a) 5%P_0 and (b) 10%P_0

Figure 7 shows the impact force which considers dynamic relaxation and without dynamic relaxation. The pier model with axial load of 10%P_0 and vehicle velocity of 80 km/h are selected to compare peak impact force. The trend of the two curves changes after the peak value of impact force occurred due to extrusion of cargo stiffness. The peak value of impact force for the model which includes dynamic relaxation into account is 4.19 MN at 0.031 s and the model without dynamic relaxation is 3.62 MN at 0.032 s which is different by 13%. The peak impact force makes the damage mode and dynamic response of the bridge pier work in a different performance. As the result, preload due to dynamic relaxation is considered in this paper to produce accurate results.
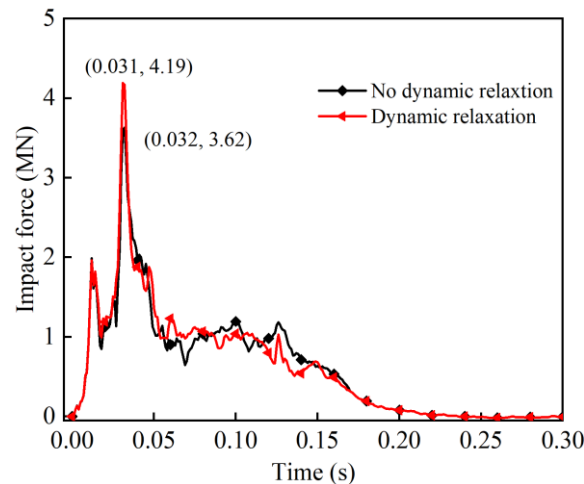

Figure 7 Impact force time history curve

4.2 COMPARISON OF PIER DYNAMIC RESPONSE

4.2.1 ENERGY ANALYSIS

The process of vehicle bridge collision is the process of energy conversion, and energy conservation is the premise to ensure the correct calculation results. Figure 8 shows the energy-time history curves calculated by each model when the impact velocity and vehicle weights are 80 km/h and 8t. At the initial time of the collision (t = 0.0 s), the total energy of the vehicle bridge collision system is the initial kinetic energy E of the vehicle. The calculation formula of the initial kinetic energy is Equation (6). After the vehicle contacts the pier, the kinetic energy begins to transform into internal energy $E_{internal}$, hourglass energy $E_{hourglass}$, sliding energy $E_{sliding}$, and other energy E_{Other}. Equation (7) is the conservation energy formula in the whole collision process. It can be seen from Figure 8 that the total energy fluctuates to a certain extent, but the fluctuation range is less than 5%, which belongs to the normal acceptable range. In addition, after the collision, most of the initial kinetic energy of the vehicle is transformed into the internal energy of the pier and vehicle deformation, accompanied by a small amount of hourglass energy, and sliding energy. However, the total energy keeps constant during the simulation and the conservation of the energy during the numerical simulation shows numerical stability of the simulation.

$$E_{total} = \frac{1}{2} m v^2 \tag{6}$$

Where: m is the total mass of the vehicle; v is vehicle collision speed

$$E_{total} = E_{internal} + E_{hourglass} + E_{slide} + E_{other} \tag{7}$$

Among them: E_{total} mainly refers to the elastic and plastic deformation energy of vehicles and piers.

$E_{sliding}$ -the energy generated by friction and damping
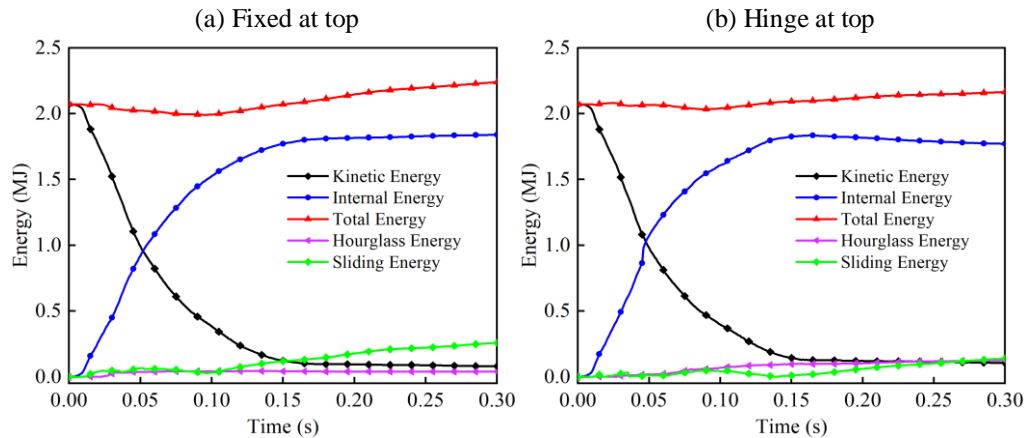
E_{other} -Collision loses energy

Figure 8 Energy time history curve (Velocity 80 km/h)

Table 5 shows the proportion of sliding energy calculated by each model is greater than that of hourglass energy. This is because Ford F800 has set up one-sided contact algorithm of its own parts and we have assigned element eroding value for material concrete and reinforcement. During the collision, the vehicle has a large deformation, which leads to the self-contact of various components of the body, and at the same time, there will be contact between various components. In addition, the vehicle and pier have face-to-face contact, and with the continuous development of vehicle deformation, the longer contact time is a large amount of interface contact slid energy will be generated. In general, the energy data calculated by each model are consistent with the basic law of energy conversion and meet the calculation requirements.

Table 5 Energy proportion of each model (Unit: joule)

Energy type / Pier model	E_{Total}	$E_{Hourglass}$	$E_{Sliding}$	$E_{Hourglass}/E_{Total}$	$E_{Sliding}/E_{Total}$
Fixed	2.24×10^6	0.04×10^6	0.26×10^6	1.78%	11.60%
Hinged	2.16×10^6	0.13×10^6	0.14×10^6	6.02%	6.48%
$5\%P_0$	2.30×10^6	0.04×10^6	0.35×10^6	1.74%	15.21%
$10\%P_0$	2.45×10^6	0.03×10^6	0.51×10^6	1.22%	20.81%

4.2.2 IMPACT FORCE

Figure 9 shows the impact force calculated by fixed, hinge, axially loaded with 5%, and 10% of the column's axial compressive capacity, P_0. The vehicle weight is 8t and the vehicle impact velocity is 60km/h, 80km/h, and 100km/h, respectively. As can be seen from Figures 9 (a), (b), and (c) at the same speed, the trend of the impact force-time history curve calculated by different models is almost similar, and with the increase in vehicle impact speed, the impact force obtained by each model increases in turn. When the speed is 60 km/h, 80 km/h, and 100 km/h, the average peak impact force is 2.11 MN, 3.75 MN, and 5.63 MN. With the increase in speed, the peak value increases by 77.73% and 51.13% respectively, and the peak growth rate decreases with the increase in speed.

Figure 9 (a), when the vehicle speed is 60 km/h, the difference between the first and second peak values of impact force of each model is small. Except for pier with hinge boundary condition, the first peak values of impact force of other models appear at 0.019 s, and the second peak value appears at 0.046 s, with a difference of 0.027 s. The duration of impact force of different models is between 0.23 s and 0.25 s. It can be seen from Figure 9 (b) that when the impact speed is 80 km/h, compared with the case of 60 km/h, the first peak value and

the second peak value of the impact force obtained by each model are quite different, and the duration of the impact force is between 0.21 s and 0.23 s. It can be seen from Figure 9 (c) that when the impact velocity is 100 km/h, the impact force presents three obvious local peaks, and the duration of impact force obtained by each model is between 0.16 s and 0.19 s. At the same time, the difference between the third peak of impact force and the second peak of impact force is small.

From observation, it is found that the maximum impact force is 2.22 MN, 4.19 MN, and 6.03 MN for the pier with applied compressive axial load $10\%P_0$ is greater than others. By comparing the different axial load levels $5\%P_0$ and $10\%P_0$ at velocities 60 km/h, 80 km/h, and 100 km/h, the impact force is 2 MN, 3.79 MN, 5.14 MN and 2.22 MN, 4.19 MN, 6.03 MN, with the increase of speed the peak impact force increased by 11%, 10.55% and 17.32%, respectively. However, the impact time for the first and second impacted force are almost the same. The high axial compressive stress on the pier delayed the tension cracks caused by vehicle impact force and therefore increased the pier's cracked stiffness, which led to higher dynamic forces. We can say that the peak dynamic force increased when the compressive axial load increased.

It can be seen that when fixed and hinge boundary conditions, the peak impact force for each condition is 1.9 MN, 3.14 MN, 5.38 MN, and 2.3 MN, 3.87 MN, and 5.43 MPa, with the increase in velocity the peak impact force increase intern by 21.05%, 23.25 and 1%, respectively. It is more obvious when vehicle velocity reaches 100km/h, the first and second impact and time do not change, but for the third impact force due to cargo stiffness, it is more clearly higher for fixed conditions. It indicates that peak values of impact force obtained from the fixed constraint of the pier are the smallest. We can assume that changing the pier's top boundary condition slightly changed the peak dynamic value because the peak dynamic value is induced in a very short period. The pier's response is controlled by the amplitude of the imposed kinetic energy as the impact duration is very small compared with the natural period of the column.

(a) Impact velocity 60 km/h
(b) Impact velocity 80 km/h
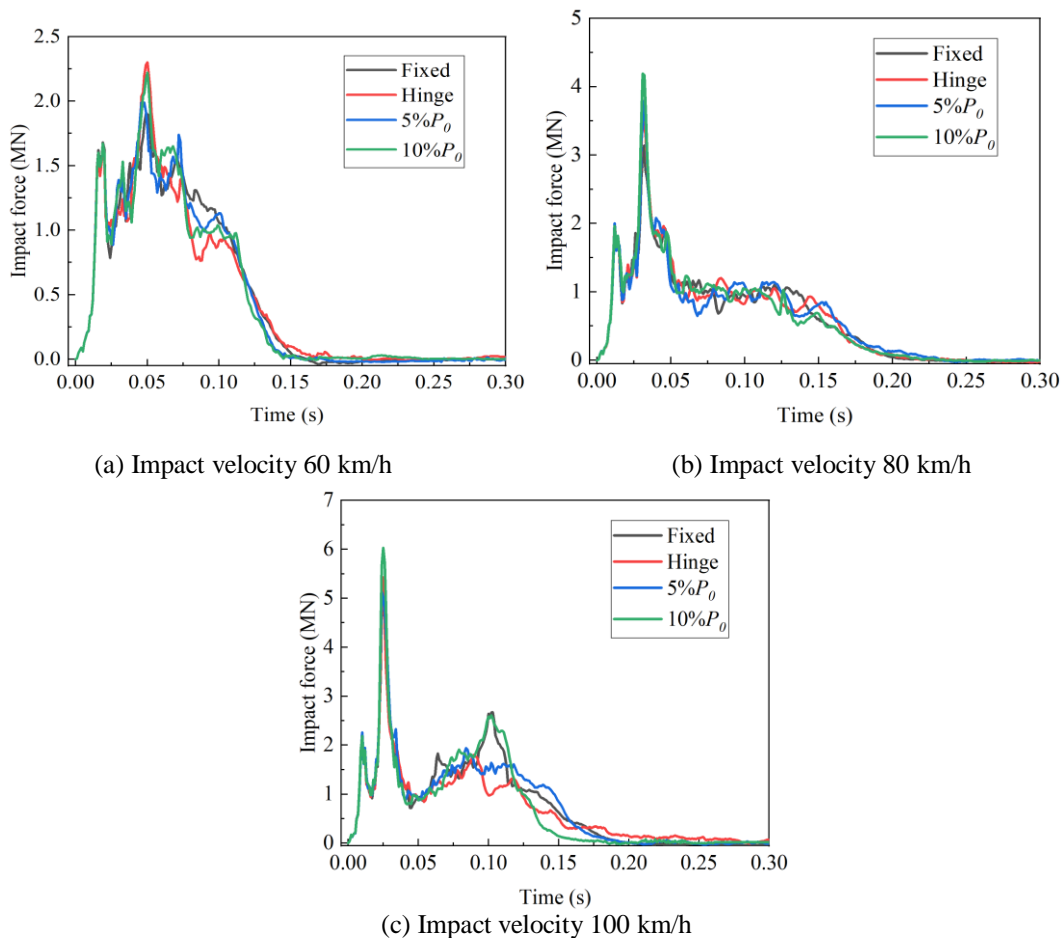
(c) Impact velocity 100 km/h
Figure 9 Impact force time history curve of each model

Figure 10 shows the comparison between the peak impact force calculated by each model and the code limit value when the vehicle weight is 8t and the impact speed is 60 km/h, 80 km/h, and 100 km/h, respectively. It can be seen that the peak impact force of each model at three speeds is about 2.1 times, 3.75 times, and 5.5 times of the limit value of the Chinese code, and about 1.2 times smaller than the AASHTO code

at speed of 60 km/h, but when the velocity reach to 80 km/h and 100 km/h, it is about 1.4 times and 2.04 times of that AASHTO code, respectively. Compared with the peak value of impact force, the limit values of impact force in Chinese and American codes are smaller. However, EI Tawail [27] believes that the peak value of dynamic impact force cannot represent the structural demands when designing because, during the time of the peak dynamic force (PDF), which is the maximum impact force of the vehicle collision with a bridge pier, the entire structure has not had enough time to respond the loading, because it lacks the time history of impact force, the equivalent static value is a better index to measure the structural design requirements because the result is not as susceptible to issues associated with hour glassing that is expected in finite element analyses.
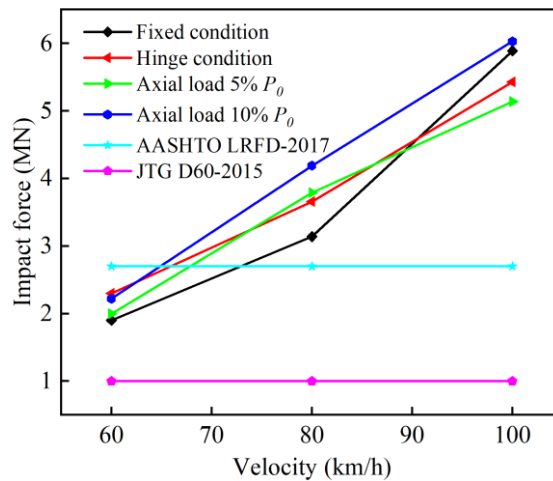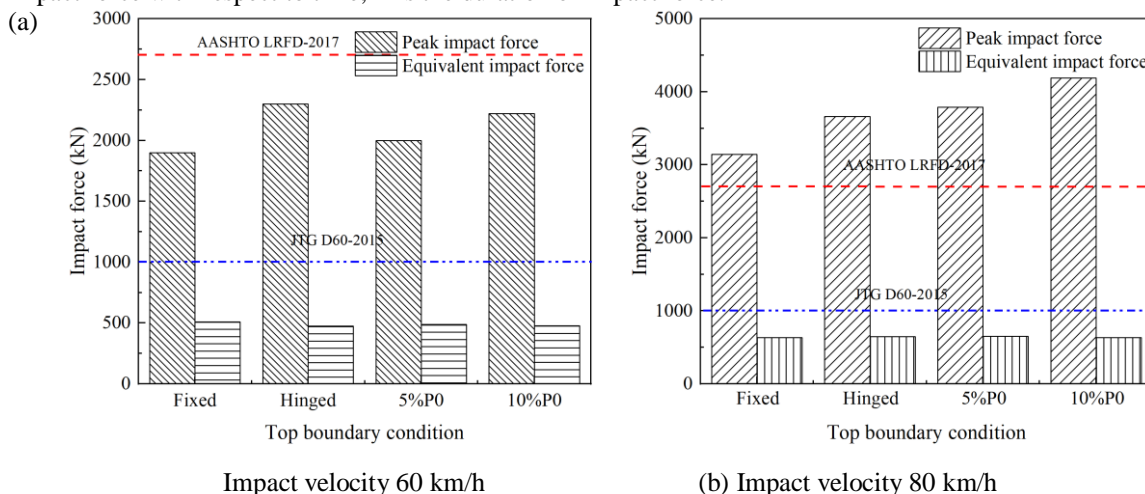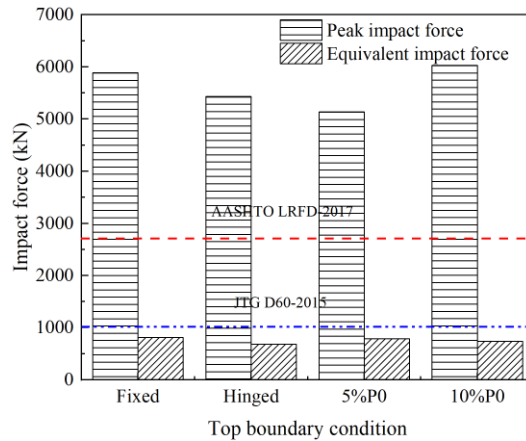

Figure 10 Comparison of peak impact force at different speeds

The equivalent static method is adopted in JTG D60-2015, which stipulates that the impact load limit of urban piers is 1000 kN [1]. As shown in Figure 11, the impact force obtained by each model at the speed of 60 km/h, 80 km/h, and 100 km/h is converted into equivalent static force by using equation (8). the peak value of impact force and the equivalent static value calculated by each model at three speeds are about 2.4 times, 4.8 times, 7.8 times, 0.7 times, 0.9 times, and 1.3 times of the code limit value respectively. Compared with the impact force peak value (PDF), the difference in the equivalent static force of each model is small. Obviously, when the vehicle speed reaches 100 km/h, the limit value of 1000 kN specified in the Chinese code is relatively small, while the limit value of impact force specified in the AASHTO code [2] is 2700kN, which is relatively conservative.

$$F_{mean} = \frac{I}{T} \tag{8}$$

Where: I is the impulse of impact force, and its calculation formula is $I = \int_{0}^{T} F(t)\,dt$, $F(t)$ is the function of impact force with respect to time; T is the duration of impact force.

(a)

Impact velocity 60 km/h
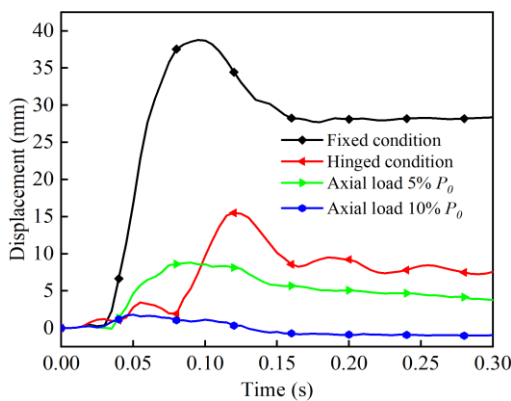
(b) Impact velocity 80 km/h
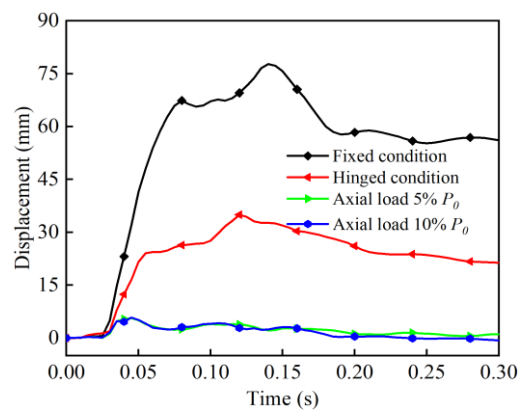
(c) Impact velocity 100 km/h

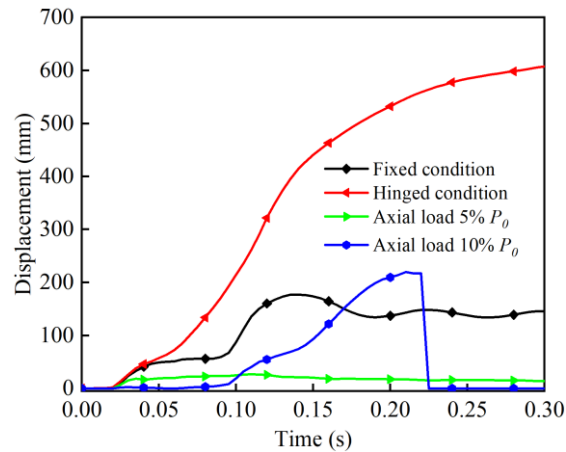Figure 11 Equivalent impact load comparison

4.2.3 PIER DISPLACEMENT

From observation made in the field, Buth [28] found that shear failure was the governing mode of failure of pier undergoing vehicle collision. Since shear tends to control the failure mode, the displacement is obtained at the time of maximum shear force generated within the pier. Figure 12 (a) (b), and (c) show the time history curves of transverse pier displacement at the height of 0.726 m when the vehicle speed is 60 km/h 80 km/h, and 100 km/h, respectively. When the impact velocity is 60 km/h, the displacement values obtained by the axial load $10\%P_0$ model are smaller than those obtained by the fixed hinge, and $5\%P_0$. The peak displacement value obtained by the $10\%P_0$ condition model is 1.8 mm, and the displacement values obtained by the fixed hinge, and $5\%P_0$ model are 38.8 mm 15.5 mm, and 8.8mm, which are about 21.6 times, 8.6 times and 4.9 times of the former, respectively. When the speed is 80 km/h, the peak displacement obtained by the model with axial load of 10% P_0 is 4.63 mm, and the model with fixed, hinge, and axial load of $5\%P_0$ is 77.7 mm, 35 mm, and 5.64 mm, which are about 16.78 times,7.6 times and 1.16 time of the former, respectively. When the speed is 100 km/h, the pier model with hinge condition collapses, due to failure in the top boundary condition, so the peak displacement is 607.88 mm, which is the corresponding value at 0.3s after the impact. At the same time, it can be seen that the pier model with the axial load $10\%P_0$ collapse due to the concrete and steel has reached the failure strain that why the curve drops down suddenly due to the element erosion, the peak displacement is 220 mm, which is the corresponding value at 0.21 s after the impact. The peak displacement for the model with fixed and $5\%P_0$ conditions is 177.4 mm and 27.1 mm. We can see that the pier with the $5\%P_0$ axial load has smaller displacement than fixed, axial load $10\%P_0$, and hinge condition, which are 6.55 times, 8.12 times, and 28 times of $5\%P_0$ condition. It shows that the boundary condition and change in axial load capacity of the superstructure has a great influence on the dynamic response of the pier after impact.

(a) Impact velocity 60 km/h

(b) Impact velocity 80 km/h

(c) Impact velocity 100 km/h
Figure 12 Time history curve of transverse displacement of pier

V. CONCLUSION

In this study, the vehicle-pier collision was established in LS-DYNA and validated. The constitutive nonlinear material model was used and validated by comparing with published result. After numerical model validation, parametric studies were carried out to analyze the effect of preload induced by implicit dynamic relaxation, compressive axial load, boundary condition at top end, and impact velocity. The peak impact force was analyzed and converted into equivalent statice force and compared with AASHTO-LRFD and JTG d60-2015. The calculation results were shown that:

(1) The stress initialization of the pier due to preload generated by implicit dynamic relaxation had higher peak impact force than the pier which did not take it into account.

(2) The dynamic responses of the pier with compressive axial load $5\%P_0$ and $10\%P_0$ were quite different. The impact force of the pier $10\%P_0$ had a larger impact force than the pier $5\%P_0$. The large axial load on the pier delayed the tension fracture caused by the impacting force, increasing the pier's crack stiffness and as the result increasing the peak impact force. The displacement of the pier was identical when impact velocity was 80 km/h, and the piers collapsed when velocity reach 100 km/h.

(3) The top boundary condition affects the dynamic responses of the pier.

(4) The peak impact force was mainly caused by the collision between the vehicle engine and bridge pier and the secondary extrusion of carriage cargo can also produce the local peak value. With the increase of vehicle impact velocity, the peak impact force increases in turn.

(5) Under the three-impact velocity of 60 km/h, 80 km/h, and 100 km/h, the equivalent static impact force obtained from each condition is smaller than the impact force limit specified in AASHTO-LRFD and JTG d60-2015.

REFERENCES

[1] Ministry of Communications of the People's Republic of China, JTG d60-2015 general code for design of highway bridges and culverts [s] Beijing: People's Communications Press, 2015.

[2] "AASHTO, AASHTO LRFD Bridge Design Specifications, Sixth Edition, American Association of State Highway and Transportation Officials, Washington, D.C.," 2012.

[3] W. F. W. M. S. B. et al. , C.E.buth, "Collision Loads on Bridge Piers: Phase 2. Report of Guidelines for Designing Bridge Piers and Abutments for Vehicle Collisions — Texas A&M Transportation Institute."

[4] A. K. Agrawal and C. Chen, "'Bridge Vehicle Impact Assessment.' Project #C-07-10, University Transportation Research Consortium, New York Department of Transportation," 2008.

[5] N. L. Gomez and A. Alipour, "Study of Circular Reinforced Concrete Bridge Piers Subjected to Vehicular Collisions," Structures Congress 2014 - Proceedings of the 2014 Structures Congress, pp. 577–587, 2014, doi: 10.1061/9780784413357.052.

[6] K. Wardhana and F. C. Hadipriono, "Analysis of Recent Bridge Failures in the United States," Journal of Performance of Constructed Facilities, vol. 17, no. 3, pp. 144–150, Aug. 2003, doi: 10.1061/(ASCE)0887-3828(2003)17:3(144).

[7] W. Cook, "Bridge Failure Rates, Consequences, and Predictive Trends," 2014.

[8] L. Chen, Y. Xiao, G. Xiao, C. Liu, and A. K. Agrawal, "Test and numerical simulation of truck collision with anti-ram bollards," International Journal of Impact Engineering, vol. 75, pp. 30–39, Jan. 2015, doi: 10.1016/J.IJIMPENG.2014.07.011.

[9]   H. Al-Thairy and Y. C. Wang, "An assessment of the current Eurocode 1 design methods for building structure steel columns under vehicle impact," Journal of Constructional Steel Research, vol. Complete, no. 88, pp. 164–171, 2013, doi: 10.1016/J.JCSR.2013.05.013.

[10]   L. Chen, S. M. Asce, ; Sherif El-Tawil, F. Sei, F. Asce, and Y. Xiao, "Reduced Models for Simulating Collisions between Trucks and Bridge Piers," 2016, doi: 10.1061/(ASCE)BE.1943.

[11]   S. El-Tawil, E. Severino, and P. Fonseca, "Vehicle Collision with Bridge Piers," Journal of Bridge Engineering, vol. 10, no. 3, pp. 345–353, May 2005, doi: 10.1061/(ASCE)1084-0702(2005)10:3(345).

[12]   G. , Liu, "Behavior of Bridge Piers during Vehicular Impact" Ph.D thesis, City College of New York, City University of New York.," 2012.

[13]   X. Xu, "'Performance based approach for loading and design of bridge piers impacted by medium weight trucks.' Ph.D. thesis, City College of New York, City University of New York," 2017.

[14]   Agrawal et al., "A Performance Based Approach for Loading Definition of Heavy Vehicle Impact Events," Report No.FHWA-HIF-18-062, 2018.

[15]   Yvonne D. Murray, "Users Manual for LS-DYNA Concrete Material Model 159," 2007.

[16]   R. Cao, S. El-Tawil, A. K. Agrawal, X. Xu, and W. Wong, "Behavior and Design of Bridge Piers Subjected to Heavy Truck Collision," Journal of Bridge Engineering, vol. 24, no. 7, p. 04019057, Jul. 2019, doi: 10.1061/(asce)be.1943-5592.0001414.

[17]   J. O. Hallquist, "Hallquist, J.O. (2006) LS-DYNA Theory Manual. Livermore Software Technology Corporation (LSTC), Livermore. - References - Scientific Research Publishing."

[18]   C. Zener, J. H. Hollomon, C. Zener, and J. H. Hollomon, "Effect of Strain Rate Upon Plastic Flow of Steel," JAP, vol. 15, no. 1, pp. 22–32, 1944, doi: 10.1063/1.1707363.

[19]   L. Bu, "Simplified Dynamical Probability Method for Ship-Bridge Collision. Master dissertation [Master, thesis], Tongji University, China," 2011.

[20]   W. Juan, "The crashworthiness of the substructures of urban bridges impacted by heavy vehicles [Ph.D. thesis], Tongji University, China," 2015.

[21]   S. , & D. J. Bala, "General Guidelines for Crash Analysis in LS-DYNA. Livermore Software Technology Corporation," 2012.

[22]   J. O. Hallquist, "LS-DYNA keyword user's manual. Livermore Software Technology Corporation, 970," 2007.

[23]   "National Crash Analysis Center (NCAC)," http://www.ncac.gwu.edu.

[24]   "HEAVY VEHICLE INFRASTRUCTURE ASSET INTERACTION AND COLLISION," 2005.

[25]   K. Fujikake, B. Li, and S. Soeun, "Impact Response of Reinforced Concrete Beam and Its Analytical Evaluation," Journal of Structural Engineering, vol. 135, no. 8, pp. 938–950, Aug. 2009, doi: 10.1061/(ASCE)ST.1943-541X.0000039.

[26]   L. Chen, S. El-Tawil, and Y. Xiao, "Response spectrum-based method for calculating the reaction force of piers subjected to truck collisions," Engineering Structures, vol. 150, pp. 852–863, Nov. 2017, doi: 10.1016/j.engstruct.2017.07.092.

[27]   S. El-Tawil, M. Asce, ; Edward Severino, and P. Fonseca, "Vehicle Collision with Bridge Piers," 2005, doi: 10.1061/ASCE1084-0702200510:3345.

[28]   C. E. Buth, W. F. Williams, M. S. Brackin, D. Lord, S. R. Geedipally, and A. Y. Abu, "ANALYSIS OF LARGE TRUCK COLLISIONS WITH BRIDGE PIERS: PHASE 1. REPORT OF GUIDELINES FOR DESIGNING BRIDGE PIERS AND ABUTMENTS FOR VEHICLE COLLISIONS 5. Report Date 6. Performing Organization Code 13. Texas Department of Transportation and the Federal Highway Administration. Project Title: Guidelines for Designing Bridge Piers and Abutments for Vehicle Collisions Unclassified," 2009.